Technical Note	LIGO-T1800245–v1	2018/06/02

Optical loss characterization at the 40m prototype lab

SURF Student: Pooja Sekhar, Mentors: Gautam Venugopalan, Koji Arai

California Institute of Technology
LIGO Project, MS 18-34
Pasadena, CA 91125
Phone (626) 395-2129
Fax (626) 304-9834
E-mail: info@ligo.caltech.edu

Massachusetts Institute of Technology
LIGO Project, Room NW22-295
Cambridge, MA 02139
Phone (617) 253-4824
Fax (617) 253-7014
E-mail: info@ligo.mit.edu

LIGO Hanford Observatory
Route 10, Mile Marker 2
Richland, WA 99352
Phone (509) 372-8106
Fax (509) 372-8137
E-mail: info@ligo.caltech.edu

LIGO Livingston Observatory
19100 LIGO Lane
Livingston, LA 70754
Phone (225) 686-3100
Fax (225) 686-7189
E-mail: info@ligo.caltech.edu

http://www.ligo.caltech.edu/

1   Introduction

Albert Einstein predicted the existence of gravitational waves (GWs) through his General Theory of Relativity in 1916. As compared to electromagnetic waves, GWs have very low absorption cross-section which makes them very effective in providing information about the universe and various astrophysical events that are distinct from those obtained using electromagnetic spectrum [1]. As a result of the relentless efforts by many scientists over many decades, these waves with extremely small amplitude were discovered on September 14, 2015 by the twin detectors of aLIGO with a signal to noise ratio of 24 [2].

Although the basic technique of Michelson interferometer has been employed, several advancements including four stage suspension of test masses for seismic isolation, highly stable laser that can be boosted upto 200W, control loop mechanisms and many more have been included so that the intensity of light at the photodiode which is a function of the differential arm length ($DARM = \frac{L_X - L_Y}{2}$) of the interferometer as shown in Figure 1 gives the gravitational wave strain [3]. The test masses are made of fused silica to minimize IR absorption and optical coatings are extremely smooth to reduce scatter loss. They are also very large with a diameter of 34cm and weigh around 40kg for vibration isolation [4]. Cameras have been placed facing various optic in the interferometer for continuous observation of the beam spot on the test masses.
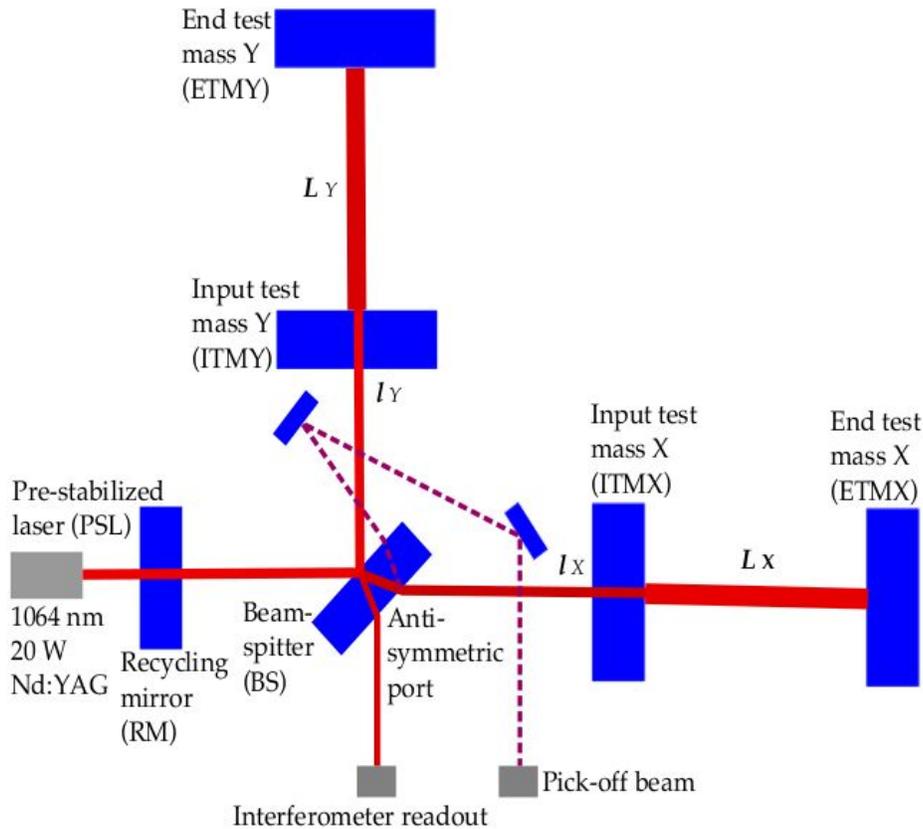
Figure 1: Gravitational wave strain is derived from differential arm motion (DARM) that is read-out from a photodiode downstream of the antisymmetric port [5]

Since closed circuit analog camera networks were associated with many disadvantages like inability to change the exposure times, digital camera networks were proposed and implemented a decade ago [6]. Later cameras with Gigabit Ethernet (GigE) connection were employed for faster data transmission over ethernet from a camera network to the computer. It provides data on position, mode and intensity fluctuations of the laser beam and through integration with the control loops of aLIGO, aid in aligning the laser beam in optical cavities. In this project, GigE cameras will be used to measure the scatter loss in optical cavities.

Being a very sensitive instrument, aLIGO is prone to a wide range of noise sources in spite of these precautions. Scattering of light, one of the noise sources, is the deflection of light from its path defined by specular reflection caused due to the irregularities on the surface of test masses. It reduces the power circulating in the Fabry perot cavities leading to a low signal to noise ratio and scattered light might also couple back into the instrument imparting random phase noise. In order to measure the scattered light, a CCD camera, Basler ace acA640-120gm, with Gigabit Ethernet (GigE) connection will be used such that it can image the test masses. Since intensity of the scattered light is angle dependent, bidirectional reflectance distribution function (BRDF) as defined below, will be employed to calibrate CCD from pixel counts to power units [7].

$$BRDF = \frac{P_s/\Omega}{P_i \ \cos(\theta_s)} \tag{1}$$

where θ_s is the scattering angle and Ω is the solid angle subtended at the sensor.

Here Lambertian model with BRDF = $\frac{1}{\pi}$ sr^{-1} has been assumed and CCD has been calibrated accordingly. The scattered power (P_s) has been calculated from the images of the calibrated CCD according to the following equation,

$$P_s = \text{Calibration Factor}(CF) \times \frac{\sum\limits_{ROI} \text{Pixel Value}}{\text{Exposure Time}} \tag{2}$$

where ROI is the region of interest selected around the beam spot in the captured images. Here the pixel counts have been summed over the ROI and normalized by the camera exposure time [7].

Thus, scattering loss in all the optical cavities can be measured using a GigE camera. The fluctuations observed in light intensity in the videos captured has been of great interest even in aLIGO since on finding the causes behind it, we can feedback loop to control the cavity parameters and thus reduce these fluctuations. In this project, we are trying to learn how to account motion of the test masses as a cause of intensity fluctuations by analyzing the videos captured using the GigE camera.

2 Objectives

- Implement appropriate two lens system that focuses the image of the optic onto the camera.

- Characterize losses in all the optical cavities of the interferometer by installing many GigE cameras that image all optics.

- Develop a good means to interface Pylon software of GigE camera, Basler ace acA640-120gm, with python to capture images and videos at a frame rate of 30-50fps.

- Develop a neural network to correlate the fluctuations in intensity of the scattered light to the motion of the test masses from ground vibrations and other means and thus to analyze the motion of beam spot and point scatterers like dust particles across the surface of the test masses from the videos captured.

3 Telescopic Lens System

Here, our objective is to focus test mass of size 3 inches and a beam spot of size 1 inch on rectangular sensor of GigE camera placed at a distance of 1m from the test mass. A schematic of the telescopic lens system with two biconvex lenses that has to be placed between the CCD camera and vacuum viewport to focus the beam spot and the optic onto the camera sensor has been shown in the figure below.

Schematic of the telescopic lens system
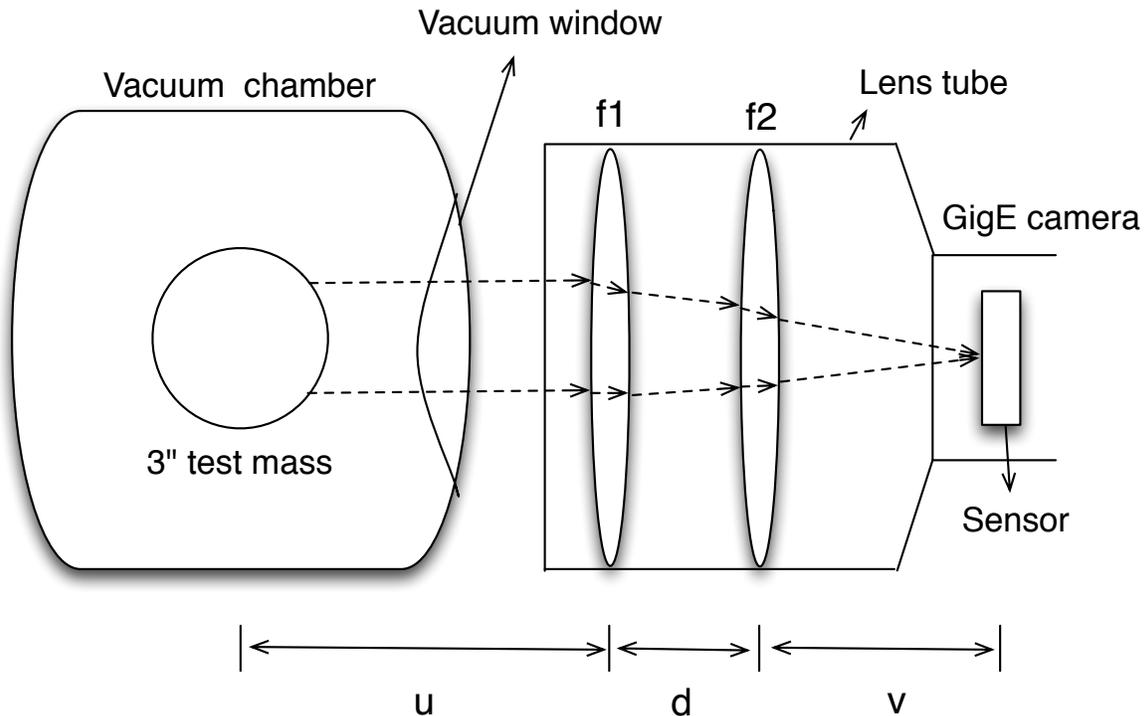
Path of light rays shown in dashed lines

ABCD matrix analysis has been employed to calculate the focal lengths of a combination of two biconvex lenses to be placed at a distance d apart so as to focus the beam spot onto the camera sensor [8]. According to this formalism, the object and the image parameters are related by the following equation,

$$\begin{bmatrix} y \\ \theta\prime \end{bmatrix} = \begin{bmatrix} 1 & v \\ 0 & 1 \end{bmatrix} \begin{bmatrix} 1 & 0 \\ \frac{-1}{f_1} & 1 \end{bmatrix} \begin{bmatrix} 1 & d \\ 0 & 1 \end{bmatrix} \begin{bmatrix} 1 & 0 \\ \frac{-1}{f_2} & 1 \end{bmatrix} \begin{bmatrix} 1 & u \\ 0 & 1 \end{bmatrix} \begin{bmatrix} x \\ \theta \end{bmatrix} \tag{3}$$

where, y and x represent the image and object heights respectively, $\theta\prime$ and θ are the angles made by the rays from image and object with the principal axis, f_1 and f_2 are the focal lengths of the lenses, v = distance of the camera sensor from the second lens, d = distance between the lenses and u = distance of the object from the first lens. The system matrix that relates the image and object parameters is as follows,

$$\begin{bmatrix} 1 & v \\ 0 & 1 \end{bmatrix} \begin{bmatrix} A & B \\ C & D \end{bmatrix} \begin{bmatrix} 1 & u \\ 0 & 1 \end{bmatrix} = \begin{bmatrix} A+Cv & u(A+Cv)+B+Dv \\ C & Cu+D \end{bmatrix} \tag{4}$$

According to the imaging criteria in paraxial approximation, light rays should converge at the image plane irrespective of the incident angle, therefore,

$$u(A+Cv)+B+Dv = 0 \tag{5}$$

$$v = \frac{-Au-B}{Cu+D} \tag{6}$$

Also, magnification (m) of the imaging system is defined as,

$$m = A + Cv = 1 - \frac{d}{f_2} + (\frac{-1}{f_1} - \frac{1}{f_2} + \frac{d}{f_1 f_2})v \tag{7}$$

The optimum image circle diameter is found to be $\frac{1}{4}$ inches such that the image circle just encloses the sensor and thus efficiently utilizes the pixels. [9] So, the required magnification is found to be 0.083 for focusing the entire optic of size 3 inches and 0.25 for the beam spot of size 1 inch. If the magnification values are greater than these respective values, some information will be lost.

Using the above formalism a Python program was developed to select the appropriate combination of focal lengths with the available options from Thorlabs such that the combination can focus the entire optic as well as the beam spot by varying the distance between the lenses (d). Here lenses with 2" diameter have been chosen to collect maximum power since the solid angle subtended on 1" lenses reduces to one-fourth of that on 2" lenses. It was found that three combinations of focal lengths served the purpose. Percentage error in magnification is defined as follows,

$$\triangle m = \frac{\text{calculated m} - \text{actual m}}{\text{actual m}} \times 100 \tag{8}$$

where actual m values are 0.083 for focusing the test mass and 0.25 for focusing the beam spot. The colorbar plots for the percentage error in magnification of 150mm-150mm, 125mm-150mm and 125mm-125mm lenses to focus the entire optic as well as the beam spot are shown

in Figures 2(a)-2(f). A sensitivity analysis was also performed and the results show that an error of 1cm in object distance and 5mm in the distance between lenses leads to a change in the error in magnification less than 3%.
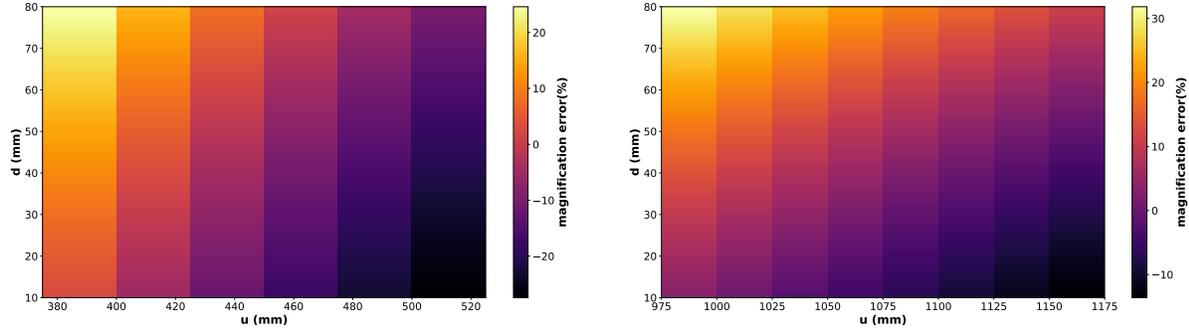
(a) 150mm-150mm combination to image 1" beam spot

(b) 150mm-150mm combination to image 3" optic
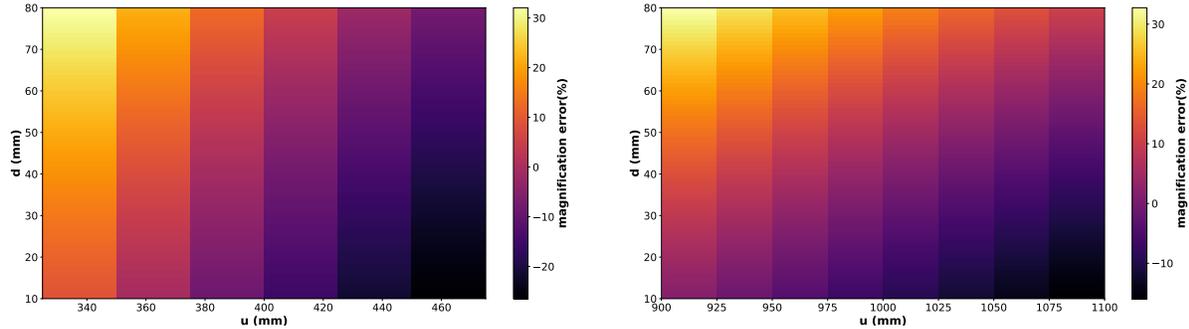
(c) 125mm-150mm combination to image 1" beam spot

(d) 125mm-150mm combination to image 3" optic
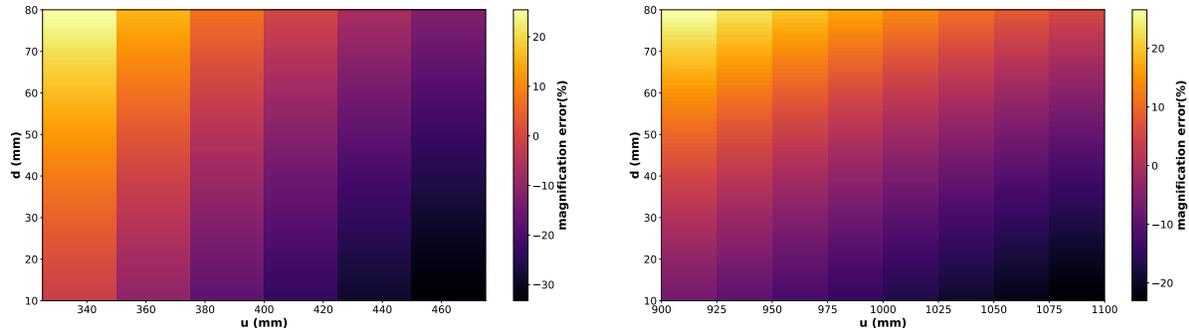
(e) 125mm-125mm combination to image 1" beam spot

(f) 125mm-125mm combination to image 3" optic

Figure 2: Colorbar plots showing percentage error in magnification for various combinations of lenses

Here we have even considered imaging the object to a size lesser than $\frac{1}{4}$ inches by approximately 8%. However, there is a practical difficulty in placing the lenses since there exists difference in the total distance between the test mass and camera of approximately 8cm, 20cm and 28cm in the two cases i.e. on focusing beam spot and test mass for solutions

of 125mm-125mm, 125mm-150mm and 150mm-150mm combinations respectively. Thus, 125mm-125mm combination may be appropriate for this purpose. However, this solution requires the lenses to be apart by 15cm and imposes a practical difficulty that we need to join many lens tubes or have a longer lens tube.

4   Neural network to analyze the video

In order to understand the involvement of motion of test masses to the intensity fluctuations in the scattered light, neural networking can be used [10]. The block diagram in Figure 3 illustrates the technique of neural networking we are planning to employ to correlate the light intensity fluctuations with the angular motion of test mass like pitch and yaw of the test mass. A sine signal of low frequency is imparted to the test mass such that it dominates over the other causes of test mass motion and a synchronized video is to be taken with GigE camera. However, we should think of ways to ensure that the video taken is synchronized with the applied signal. A Python program has to be developed to convert the video stream to image frames and the resultant 2D array of pixel values of each image has to be converted to a 1D array which has to be further divided into train and test values. The train values are then given to the neural network to be implemented in Keras [11]. It can be done using Sequential model as well as Model class API where a model can be instantiated using a given input tensor and output tensor. In the case of sequential model, we assume the number of layers and its size initially and then the model is compiled and trained to fit to the applied sine signal. The resultant error is to be minimized by choosing an appropriate optimization algorithm that updates the weights of inputs via backpropagation. Moreover, the number of epochs (number of times the entire dataset passes through the neural network) and batch size (number of batches onto which the dataset is to be divided) have to be chosen considering the time for training and convergence. Finally the test data result from the trained neural network is compared with the applied signal to give the figure of merit of the process.

5   Work to be done and Challenges

- Trying to interface Pylon software of the GigE camera using python wrapper, PyPylon, and be able to capture video streams at a frame rate of 30-50 fps.

- Employ a good means to obtain a synchronized video of the beam spot with the applied perturbation to the test mass.

- Develop a python program that can convert the captured videos to image frames.

- Find the best optimizer function in Keras that can update the weights to minimize the error and then to test its accuracy.
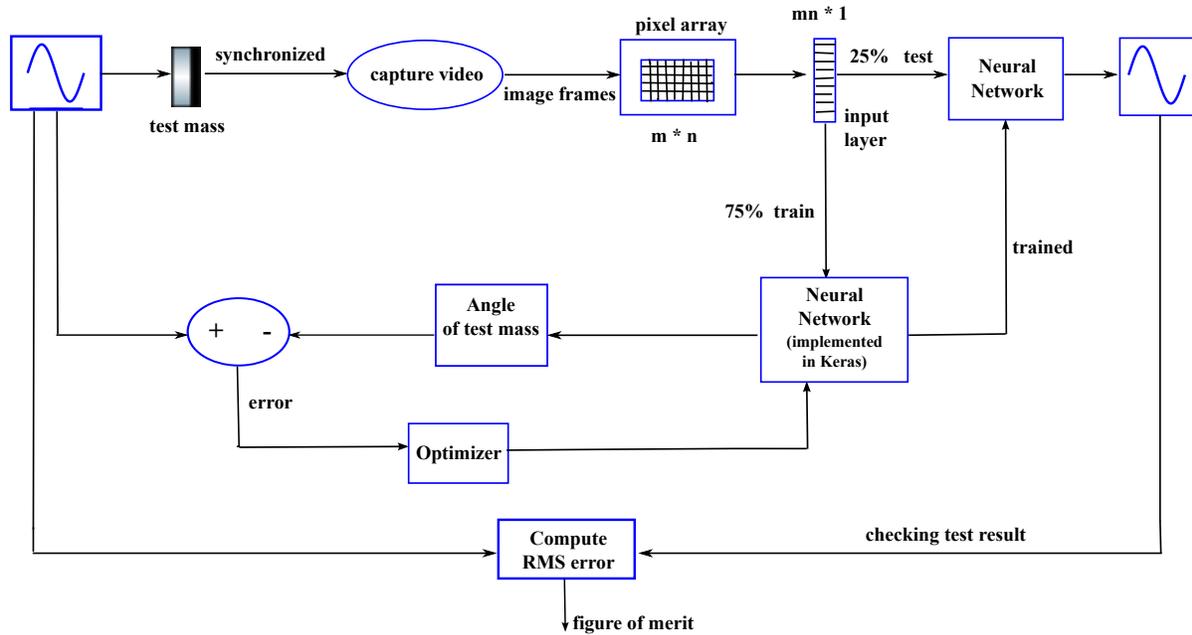
Figure 3: Block diagram that illustrates the scheme of estimating angular motion of test mass using neural network

References

[1] David G Blair, *The Detection of Gravitational Waves.* Cambridge university press (2005).

[2] B. P. Abbott *et. al.*, *Observation of Gravitational Waves from a Binary Black Hole Merger.* Phys. Rev. Lett. 116, 061102 (2010).

[3] https://www.ligo.caltech.edu/page/ligo-technology

[4] https://www.ligo.caltech.edu/page/optics

[5] Grant David Meadors, Keita Kawabe, Keith Riles *Increasing LIGO sensitivity by feedforward subtraction of auxiliary length control noise.* Classical and Quantum Gravity 31, 10 (2014).

[6] Rana Adhikari, Joseph Betzwieser, Alan Weinstein *Development of a digital camera network and associated analytical tools for the Caltech 40m LIGO prototype.* Ligo Paper (2008).

[7] Fabian Magana-Sandoval, Rana Adhikari, Valera Frolov, Jan Harms, Jacqueline Lee, Shannon Sankar, Peter R. Saulson and Joshua R. Smith *Large-angle scattered light measurements for quantum-noise filter cavity design studies.* Technical Note LIGO-T1400252-LSC (2014).

[8] Ajoy Ghatak, Optics.4th Edition (2009)

[9] Jigyasa Nigam, Mentors: Gautam Venugopalan, Johannes Eichholz *Characterization of Test Mass Scattering*. LIGO-SURF Report (2017).

[10] http://neuralnetworksanddeeplearning.com/chap1.html

[11] https://keras.io/